Antenna Cluster for Spacecraft High Effective Isotropic Radiated Power (EIRP) Applications

R. C. Clauss,[1] R. B. Lovick,[2] N. R. Mysoor,[1] and J. Zitzelberger[1]

A concept using a closely packed array (cluster) of transmit antennas for spacecraft applications that require high effective isotropic radiated power (EIRP) is described and analyzed. The September 2003 baseline Jupiter Icy Moons Orbiter (JIMO) plan information provided to this study specifies that a data rate of 10 megabits per second (Mbps) be sent from Jupiter to Earth, at a maximum distance of 6.25 AU using a 32-GHz (Ka-band) downlink with a 3-dB margin, to be received by the equivalent of a DSN 70-m antenna. This requires a 250-MW EIRP, to be delivered by power combined from four 150-W power amplifiers into a 3-m-diameter antenna. The JIMO mechanical pointing error was specified to be ±0.003 rad, which results in an EIRP loss of between 10 dB and 15 dB if a single 3-m-diameter antenna is used without some additional form of beam steering to correct for the mechanical pointing error. A cluster of four 1.5-m-diameter antennas can electronically steer a spatially combined beam to correct for the mechanical pointing error and reduce the maximum pointing loss to 2.7 dB. Pointing information for electronic beam steering may be obtained by tracking an uplink microwave signal with the cluster or from infrared or optical Earth, Sun, or star trackers mounted with the antenna cluster.

The results of a trade study comparing the single-antenna approach with the antenna-cluster approach are given, using a cluster of four antennas. The system architecture and the high-EIRP cluster concept are described. Advantages of the cluster concept over a single antenna include electronic beam steering, reduced antenna mass, higher antenna efficiency, lower power density in the transmit system components, spatial power combining, and graceful degradation.

---

[1] Spacecraft Telecommunications Equipment Section.

[2] Telecommunications Science and Engineering Division.

The research described in this publication was carried out by the Jet Propulsion Laboratory, California Institute of Technology, under a contract with the National Aeronautics and Space Administration.

I. Introduction

Future NASA deep-space mission plans call for significant data-rate increases from spacecraft at interplanetary distances to Deep Space Network (DSN) antennas. For example, the September 2003 baseline Jupiter Icy Moons Orbiter (JIMO) plan information provided to this study specifies 10-megabit per second (Mbps) data rates, generated in the vicinity of Jupiter at a distance of 6.25 AU, transmitted to the equivalent of a 70-m DSN antenna with a 3-dB margin at 32 GHz (Ka-band).[3] Combining the output of four 150-W Ka-band traveling-wave tube amplifiers (TWTAs) for use with a 3-m antenna is proposed in the JIMO plan and provides the effective isotropic radiated power (EIRP) needed to meet requirements. The JIMO spacecraft's mechanical capability to point its antenna to within ±0.003 rad (±0.172 deg) is not sufficiently accurate to meet communication-link requirements and results in excessive pointing loss at the mechanical pointing extremes. (Note that DSN 70-m antennas are not equipped to receive Ka-band signals at this time. An array of four DSN 34-m beam-waveguide antennas (such as DSS 25) is considered to be a 70-m-antenna equivalent for the purposes of this article.)

A study to use a closely packed array, or cluster, of antennas to increase spacecraft transmitter EIRP was supported by the Interplanetary Network Directorate (IND) Technology Office during fiscal year (FY) 03 and FY 04. Electronic beam steering can be accomplished by using a cluster of antennas, with the signal phase to each antenna adjusted to properly steer the spatially combined beam. Electronic beam steering results in a reduction of pointing loss and appears to be ideal for the JIMO application.

Steering the transmit antenna beam to the DSN receiving antennas on Earth to compensate for spacecraft mechanical pointing errors depends upon knowledge of the Earth's position with respect to the transmit antenna's alignment. Information about the Earth's position can be obtained from an uplink signal or by using infrared or optical Earth, Sun, or star trackers mounted on the antenna structure.

This article presents an adaptation of the antenna-cluster principles developed by the High EIRP Study Team for the JIMO application and for other future deep-space missions.

II. Transmit Antenna Array

A. Array Characteristics

As is stated in [1, pp. 689–690], "The basis for all directivity control in antenna arrays is wave interference. By providing a large number of sources of radiation, it is possible with a fixed amount of power greatly to reinforce radiation in a desired direction while suppressing the radiation in undesired directions. The individual sources may be any type of antenna."

The performance of an array of transmit antennas is determined by the individual sources (array elements) in the array. The array elements in this article are identical 1.5-m, clear-aperture, high-efficiency reflector antennas mounted on a common structure so that all elements point in the same direction. This direction is identified as the array's mechanical boresight direction. The maximum transmit intensity of each element of the array is determined by its effective area and the transmitter power delivered to each element.

Any number of transmitting elements might be used to form a transmit array. The optimum number depends upon many considerations, including the EIRP requirement, the available transmitter power levels, and the electronic beam-steering needs. The array described in this article consists of a cluster of four closely spaced antennas. A 150-W TWTA is connected to each array element.

---

[3] J. Hilland, *Technical Baseline Review-1 (TBR-1) for Jupiter Icy Moon Orbiter Telecom Subsystem* (internal document), Jet Propulsion Laboratory, Pasadena, California, September 2003.

B. Radiation Patterns

The transmit intensity of each element varies as a function of the angle between the target and the array's mechanical boresight direction. The half-power beamwidth (HPBW) of a high-efficiency, uniformly illuminated, circular reflector antenna is close to a value that is equal to the wavelength divided by the diameter, in radians. The beamwidth between the first nulls of the radiation pattern is 2.4 times the HPBW.

Knowledge of each transmitting element's radiation pattern is needed to determine the EIRP levels associated with pointing errors. Theoretical patterns of circular reflector antennas can be determined from equations found in various publications [1–3,5], including the chapter on spacecraft antennas by Rahmat-Samii and Noreen in [2], wherein Table 8-2 shows the characteristics of tapered circular aperture distribution [2, p. 429]. The HPBW varies from 1.01 (wavelength divided by diameter, in radians) to 1.32 (wavelength divided by diameter, in radians) for different aperture distributions as the edge illumination varies from 0 dB to −20 dB.

A 3-m high-efficiency (over 80 percent) antenna with a uniform illumination pattern at 32 GHz will have an HPBW close to 0.00316 rad (0.181 deg). A 3-m antenna with 60 percent efficiency, a normal (not shaped) illumination pattern, and an edge illumination of −10 dB at 32 GHz will have an HPBW close to 0.0036 rad (0.206 deg). Antennas with 1.5-m diameters will have HPBW values that are twice those of the 3-m-diameter antennas [4].

A 3-m antenna with uniform aperture illumination, but with low efficiency caused by random surface errors in the reflector, will have approximately the same HPBW as a high-efficiency antenna of the same diameter. The random surface errors of the main reflector cause transmitted energy to be lost into the side lobes without widening the HPBW.

The EIRP of an individual element is proportional to the square of the element's intensity. The EIRP(max) in the mechanical boresight direction is the element's transmitter power multiplied by the element's antenna gain, $\left[G(\max)\right]$; 10 times the logarithm of the antenna gain ratio is used to express the antenna gain in decibels.

From [2, pp. 420–421], antenna gains are calculated using the following equations:

$$G_{\mathrm{db}} = 10 \log_{10} G \tag{1}$$

and

$$G = (\text{aperture efficiency}) \times \left(\frac{4 \times \pi \times A}{\text{wavelength}^2} \right) \tag{2}$$

This can also be written as

$$G = (\text{aperture efficiency}) \times \left[\frac{\pi \times D}{\text{wavelength}} \right]^2 \tag{3}$$

As an example, using an 80 percent efficient 1.5-m-diameter array element at 32 GHz, where a wavelength is 9.3685 mm, $G = 202,409.5$. The array element radiates a 30.36-MW EIRP in the mechanical boresight direction when a transmit power of 150 W is delivered to the array element.

When $G = 202,409.5$, $G_{\mathrm{db}} = 53.0623$ dB; 150 W is equal to 21.761 dBw or 51.761 dBm. The element's EIRP can be expressed as the sum of the element gain in decibels and the power level in dBw or dBm,

giving +74.823 dBw or +104.823 dBm, respectively. Later in this article, we will use the convenience of adding decibels, rather than multiplying power levels and gain ratios, to determine the cluster antenna transmit performance.

Each element's gain pattern, $G(\beta)$ in decibels, as a function of β, the angle off of the boresight direction, is closely approximated by the equation

$$G(\beta)\ \text{dB} = 10\log\left\{\left[G(\text{max})\right] \times \left[\cos(74.9346\ \text{deg} \times P_E)\right]^3\right\} \tag{4}$$

where P_E is β divided by the antenna HPBW.

The pattern of the cluster of four closely spaced elements is calculated [2] using Eq. (4).

The phase centers of four closely spaced 1.5-m-diameter circular apertures form a square. At 32 GHz, the intensity equation used for the directions along the diagonals of the square is

$$F_D(\beta) = 4\cos\beta\left[\cos^2\left(\frac{S^\circ}{2\sin\beta}\right)\right] \tag{5a}$$

where $F_D(\beta)$ is the intensity, β is the angle off of the boresight direction, and S° is one-half the distance between the phase centers of the diagonally opposite antennas in degrees. In this case, Eq. (5a) becomes

$$F_D(\beta) = 4\cos\beta\left[\cos(20366\sin\beta)\right]^2 \tag{5b}$$

When β equals 0.000 deg, the intensity is four times the maximum intensity of one element. EIRP varies as the intensity squared, so the maximum EIRP of the four-element cluster is 16 times the EIRP of a single element.

The EIRP increase of 16 (12.04 dB) for the array is the result of a 6.02-dB antenna array gain increase and a 6.02-dB transmitter power increase. The antenna array gain change in decibels with respect to the gain of a single element is

$$\Delta G_{\text{dB}} = 10\log\left\{4\cos\beta\left[\cos(20366\sin\beta)\right]^2\right\} \tag{5c}$$

When the angle off of the boresight direction, β, equals 0.09218 deg, the EIRP is 8 times the EIRP of a single element. This half-power point shows that the cluster's HPBW is 0.18436 deg in the direction along the diagonal of the square formed by the four elements' phase centers.

At 32 GHz, the intensity equation to be used for the directions along the edges of the square (45 deg away from the diagonals) is

$$F_E(\beta) = 4\cos\beta\left[\cos\left(\frac{S^\circ}{2\sin\beta}\right)\right] \tag{6a}$$

where $F_E(\beta)$ is the intensity, β is the angle off of the boresight direction, and S° is the distance between the phase centers of the adjacent antennas in degrees. In this case, Eq. (6a) becomes

$$F_E(\beta) = 4\cos\beta\big[\cos(28820\sin\beta)\big] \tag{6b}$$

The antenna array gain change in decibels with respect to the gain of a single element is

$$\Delta G_{\mathrm{dB}} = 10\log\big\{4\cos\beta\big[\cos(28820\sin\beta)\big]\big\} \tag{6c}$$

When $\beta = 0.08946$ deg in the direction along the edge of the square, the EIRP is 8 times the EIRP of a single element, and the cluster's HPBW in this direction is 0.17892 deg.

These HPBW values are very close to the 0.181-deg HPBW of a 3-m high-efficiency antenna (over 80 percent) with a uniform illumination pattern at 32 GHz.

The sum (in decibels) of Eqs. (4) and (5b) is used to determine the four-antenna cluster pattern along the "diagonal" direction. The sum (in decibels) of Eqs. (4) and (6b) is used to determine the four-antenna cluster pattern along the "edge" direction. The antenna cluster gain pattern for the edge direction is shown in Fig. 1, along with the gain pattern for a single element.

C. Electronic Beam-Steering Capabilities and Pointing-Loss Corrections

The antenna cluster's electronic beam-steering capability (see Fig. 2) can reduce the pointing loss caused by a mechanical pointing error. For example, the cluster's electronic beam-steering capability can reduce the pointing loss caused by a mechanical pointing error of 0.0015 rad from 2.691 dB to 0.638 dB. The Ka-band radiation pattern of the cluster of four 1.5-m antennas is shown with no electronic beam steering and with 0.0015-rad electronic beam steering in Fig. 2.

The 3-meter antenna with a 600-W power amplifier system produces a 486-MW EIRP at its beam peak. A cluster of four 1.5-m antennas, each with a 150-W power amplifier, also produces a 486-MW EIRP at the spatially combined beam peak. Table 1 shows the EIRP of these two configurations adjusted for the pointing loss caused by the mechanical pointing errors in the spacecraft system, with the EIRP recovery that results from the electronic beam-steering capability of the four-antenna cluster. The advantage of the cluster over the larger single antenna is shown in decibels.

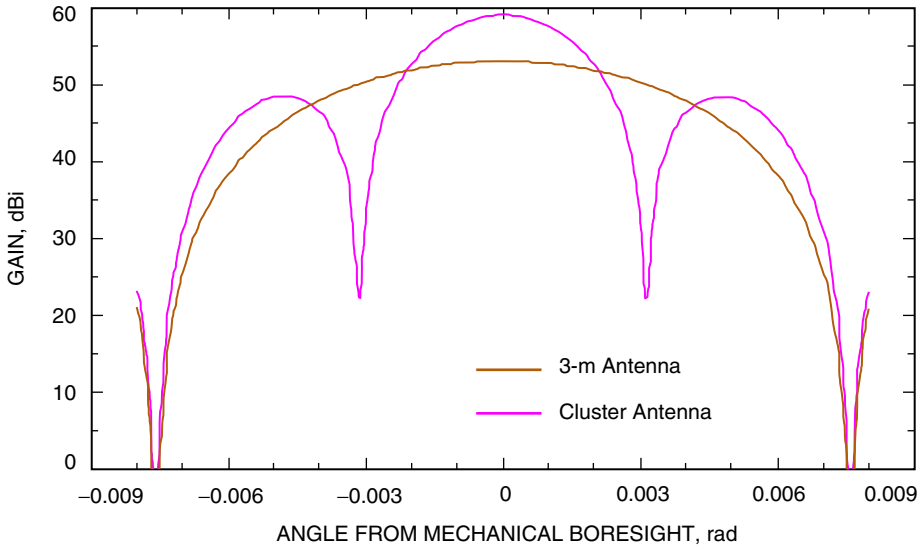

Fig. 1. Ka-band radiation pattern of a cluster of four 1.5-m antennas compared with that of a single 1.5-m antenna.

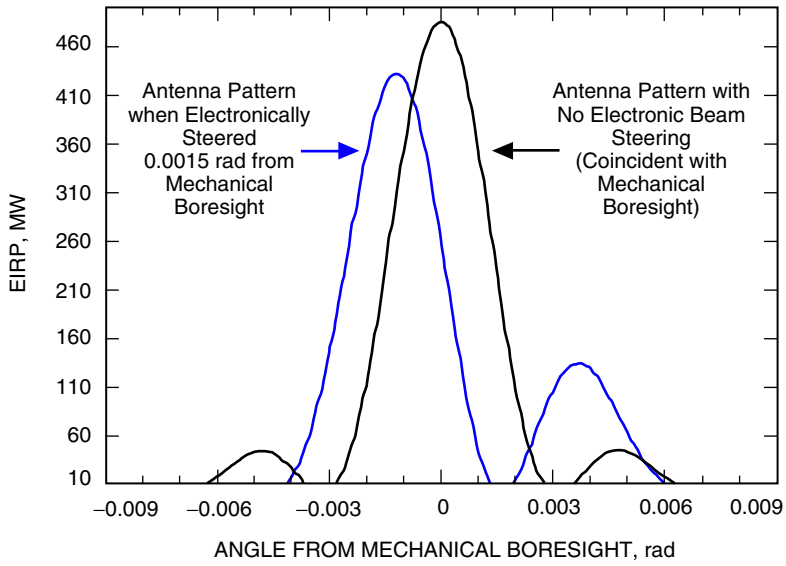

Fig. 2. Ka-band radiation pattern of a cluster of four 1.5-m antennas with and without electronic beam steering.

Table 1. EIRP versus mechanical pointing error for a 3-m antenna and for antenna clusters with electronic beam-steering EIRP recovery.

Mechanical pointing error, rad (deg)	3-m antenna EIRP, MW	4-antenna cluster with electronic beam steering, EIRP, MW	Advantage of 4-antenna cluster over 3-m antenna, dB
0.0000 (0.000)	486	486	0
0.0005 (0.029)	456	478	0.205
0.001 (0.0573)	373	456	0.873
0.0015 (0.086)	262	420	2.05
0.002 (0.1146)	150	373	3.96
0.0025 (0.143)	65	319	6.91
0.003 (0.172)	16	262	12.14

Figure 3 shows the difference in capability between a single 3-m-diameter antenna without beam-steering capability and a cluster of four 1.5-m antennas having steering capability. The maximum EIRP of the cluster would be affected by the mechanical pointing error as severely as the maximum EIRP of the single 3-m antenna if electronic beam steering were not used to correct for the mechanical pointing error. The antenna pattern of an individual element of the cluster determines the EIRP envelope as a function of the mechanical pointing error.

D. Phase Errors and Graceful Degradation

The maximum EIRP of the four-antenna cluster can be degraded by phase errors in the transmitter system and by degradation or failure of components. The graceful degradation of a system is sometimes identified as a "fail-soft" feature.

In [3], Kummer explains array theory in detail and provides a phasor presentation of pattern summation that is not repeated here. An attempt to provide a simple explanation follows.

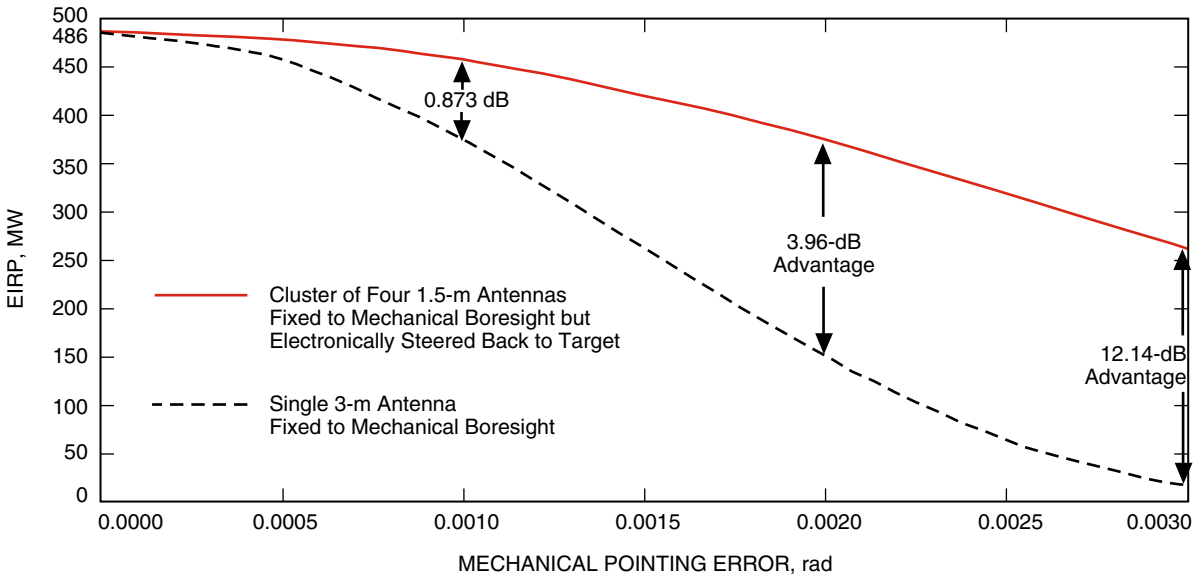

Fig. 3. Maximum EIRP versus mechanical pointing error.

The effect of phase errors and component degradation is evaluated by using a simplified form of the intensity equations, Eqs. (5a) and (6a). When no electronic steering is needed and β equals zero, both equations reduce to

$$\text{intensity}_{(D)} = 4 \tag{7}$$

The intensity of the spatially combined beam is 4 times the maximum intensity of one element. In the far field, the spatially combined relative intensity, $I_{(c\text{-}rel)}$, is the sum of the co-aligned vector components of the relative intensity of the four transmitting elements. This summation of the vectors (phasors) is most easily computed by using the angle of the vector summation as a phase reference. The sum of the sines of the error angles, $\Delta_{(1)}, \Delta_{(2)}, \Delta_{(3)}$, and $\Delta_{(4)}$, between the reference phase angle and the individual vector phase angles is zero.

The summation of the vectors, $I_{(\text{sum})}$, is

$$I_{(\text{sum})} = \left[\left(I_{(1)} \times \cos\Delta_{(1)}\right) + \left(I_{(2)} \times \cos\Delta_{(2)}\right) + \left(I_{(3)} \times \cos\Delta_{(3)}\right) + \left(I_{(4)} \times \cos\Delta_{(4)}\right)\right] \tag{8}$$

$I_{(1)}, I_{(2)}, I_{(3)}$, and $I_{(4)}$ are the relative intensities of the four transmitting elements, and $\Delta_{(1)}, \Delta_{(2)}, \Delta_{(3)}$, and $\Delta_{(4)}$ are the phase-angle differences (errors), in degrees, between each of the transmitting elements and the reference phase angle.

The loss in decibels, $L_{(\text{dB})}$, associated with transmitting-system phase-angle errors becomes

$$L = 10\log\left(\frac{\left[\left(I_{(1)} \times \cos\Delta_{(1)}\right) + \left(I_{(2)} \times \cos\Delta_{(2)}\right) + \left(I_{(3)} \times \cos\Delta_{(3)}\right) + \left(I_{(4)} \times \cos\Delta_{(4)}\right)\right]^2}{16}\right) \tag{9}$$

Table 2 shows the results of a uniform phase-angle difference between each of the transmitting elements, $\Delta_{(1)} = \Delta_{(2)} = \Delta_{(3)} = \Delta_{(4)}$, and with equal element intensities. The difference between the reference phase angle and $\Delta_{(1)}$ is negative 1.5 times the difference between each element. The difference between

Table 2. Phase-error degradation.

Phase difference between elements, deg	Phase difference between $\Delta_{(1)}$, $\Delta_{(4)}$, and reference, deg	Phase difference between $\Delta_{(2)}$, $\Delta_{(3)}$, and reference, deg	Loss, dB
0	0	0	0
2	−3, +3	−1, +1	0.0066
4	−6, +6	−2, +2	0.0265
6	−9, +9	−3, +3	0.0596
8	−12, +12	−4, +4	0.1061
10	−15, +15	−5, +5	0.1661
12	−18, +18	−6, +6	0.2396
14	−21, +21	−7, +7	0.3269
16	−24, +24	−8, +8	0.4281
18	−27, +27	−9, +9	0.5435
20	−30, +30	−10, +10	0.6733
22	−33, +33	−11, +11	0.8178
24	−36, +36	−12, +12	1.037
30	−45, +45	−15, +15	1.551
40	−60, +60	−20, +20	2.855
50	−75, +75	−25, +25	4.693
60	−90. +90	−30, +30	7.270
70	−105, +105	−35, +35	11.052
80	−120, +120	−40, +40	17.522
88	−132, +132	−44, +44	32.005

the reference phase angle and $\Delta_{(2)}$ is negative 0.5 times the difference between each element. The difference between the reference phase angle and $\Delta_{(3)}$ is positive 0.5 times the difference between each element. The difference between the reference phase angle and $\Delta_{(4)}$ is positive 1.5 times the difference between each element. The loss caused by phase-angle errors of 8 deg between each element and the reference phase will be less than 0.1 dB.

Table 3 shows the EIRP degradation that results because of a power loss of one transmitting element, with a maximum phase error of 8 deg between the reference phase angle and the phase angle of each element. The degradation is shown in decibels.

III. JIMO High-EIRP Telecommunication System Description

A proposed JIMO high-EIRP telecommunication system is presented in block diagram form in Fig. 4. In the appendix, Figs. A-1 and A-2 provide more details of this system, separating it into the components contained in the spacecraft bus and those mounted on a gimbaled antenna platform. A more detailed description follows (referring to these figures).

A. Spacecraft Telecommunication Subsystem (Fig. A-1)

1. X-Band Transmitter/Receiver (X-Band Uplink 7.145 to 7.19 GHz; X-Band Downlink 8.4 to 8.45 GHz). Cross-strapped small deep-space transponders (SDSTs), X-band TWTAs, and diplexers provide two redundant X-band transmit/receive signal chains to feeds on two of the four

Table 3. Degradation due to power loss of one element, including 8-deg phase-angle errors between the reference and the individual elements.

Single-element power, W	Combined EIRP, MW	Loss, dB
150	481	0.085
140	473	0.118
130	465	0.196
120	456	0.277
110	447	0.363
100	438	0.452
90	428	0.549
80	418	0.651
70	408	0.762
60	397	0.882
50	385	1.015
40	372	1.164
30	357	1.337
20	340	1.546
10	319	1.827
0	271	2.544

high-gain antennas (HGAs) in the antenna-structure-mounted cluster. Coaxial and waveguide transfer switches allow either of these chains to be routed to the bus-mounted medium-gain antenna (MGA) and low-gain antenna (LGA) systems instead of the HGA.

2. Ka-band Transmitter (31.2 to 32.3 GHz). Each SDST is equipped with a Ka-band modulator output [6–8]. Either transponder output can be switched to the HGA system mounted on the antenna structure.

B. Electronic Beam-Steering Assembly (Fig. 4)

The electronic beam-steering assembly consists of a monopulse tracking circuit and an electronic beam-steering circuit, and it provides the tracking and pointing functions for the Ka-band cluster array. Phase errors in the received X-band uplink signal, caused by the cluster's mechanical pointing errors, are detected by the X-band monopulse detector system. The error signal voltages then are used to determine the appropriate phase correction to properly point the Ka-band downlink signal.

In Fig. 4, the Ka-band transmit signal originating at the transponder is passed through hybrids for cross-strapping and power-dividing purposes. The signal thus is split into four identical amplitude- and phase-matched channels. Each channel is individually processed through a phase shifter, monolithic microwave integrated circuit (MMIC) amplifier, Ka-band TWTA, and antenna feed so that electronic steering of the spatially resultant beam is accomplished. The signal phase and amplitude from each of the four Ka-band TWTAs is sampled using a 35-dB coupler and compared against a reference signal using a phase comparator circuit. The error voltages at the output of the phase comparator are used to adjust the dc-offset phases in each channel to compensate for any phase drifts among TWTA and MMIC amplifiers. This will ensure precise phase-matched array channels.

To achieve the needed phase stability, transmission line lengths from the electronics assembly, through the TWTAs, and out to each antenna must be kept at a minimum. Placing the four Ka-band TWTAs

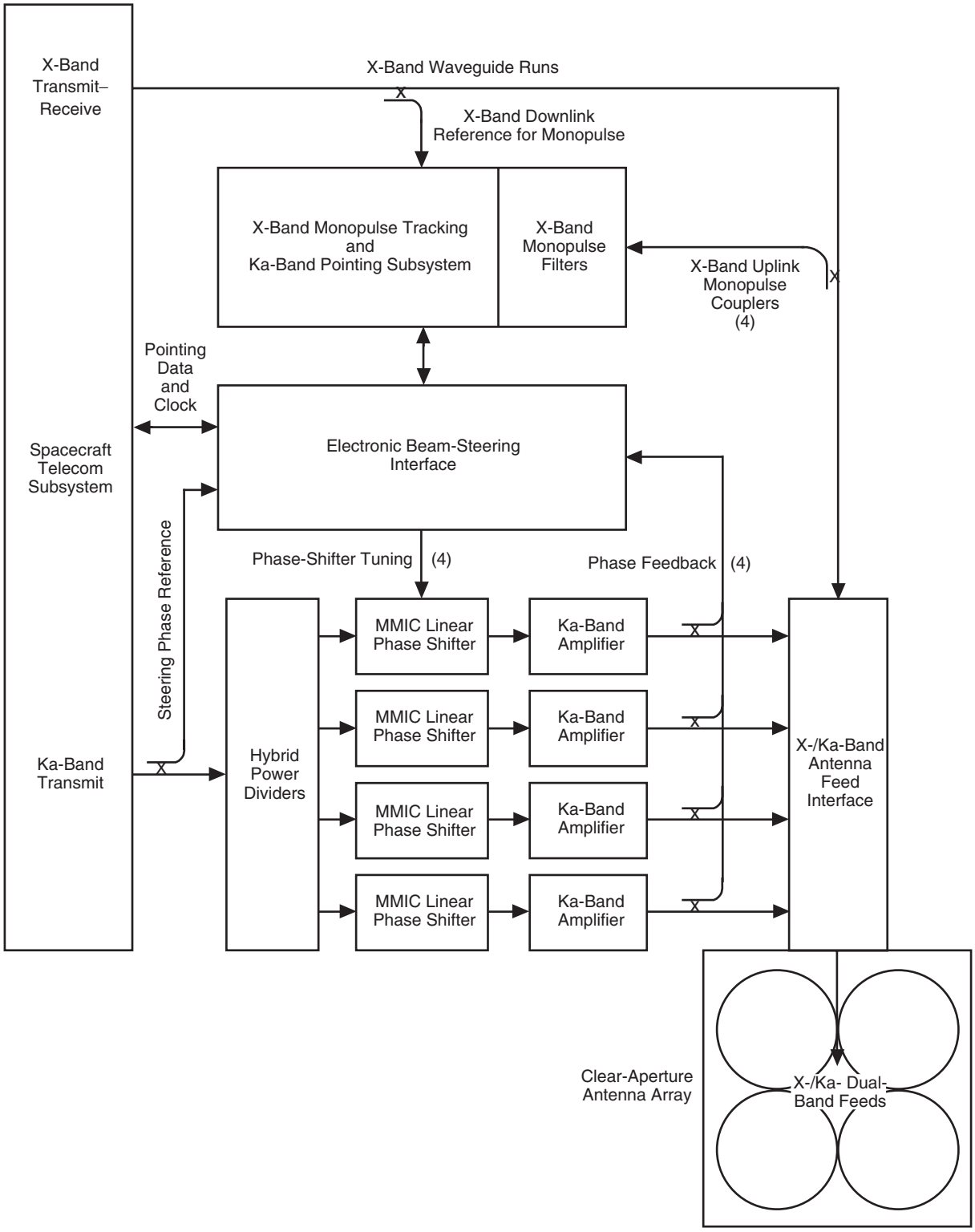

Fig. 4. High-EIRP X-/Ka-band array concept using four antennas.

on the antenna assembly just behind the cluster of antennas accomplishes this. Each Ka-band TWTA requires a separate high-voltage power supply (HVPS) whose cable cannot exceed 1-meter length, which necessitates positioning these supplies on the moveable antenna structure along with the TWTAs.

The X-band monopulse tracking unit [8,10,11] is illustrated in Fig. 5. It is used to obtain the elevation and azimuth angle errors. The signals received by each of the four antennas are represented by A, B, C, and D, respectively. The hybrid comparator configuration [9,10] utilizes phasor additions and subtractions of the received RF signals to produce the output sum pattern [$\sum_{\text{sum}} = (A + B + C + D)$], the elevation difference pattern [$\Delta_{elev} = (A+B)-(C+D)$], the azimuth difference pattern [$\Delta_{azim} = (A+C)-(B+D)$], and the diagonal difference pattern [$\Delta_{diag} = (A + D) - (B + C)$] signals. The sum and the difference channel signals are downconverted to a lower intermediate frequency (IF) signal (1.2 GHz) using a stable X-band (8.4-GHz) dielectric resonator oscillator (DRO).

The monopulse system DRO is designed to operate in both lock mode in the presence of the downlink signal from the SDST and unlock mode when the downlink signal is not present. An automatic gain control (AGC) circuit is used in the sum channel to maintain a constant reference signal level. The sum channel IF signal is used as the reference signal to the two phase detectors to produce the elevation-angle-error and azimuth-angle-error voltages [10]. These angle-error voltages are further processed in the micro-controller circuit to generate the appropriate phase correction at Ka-band.

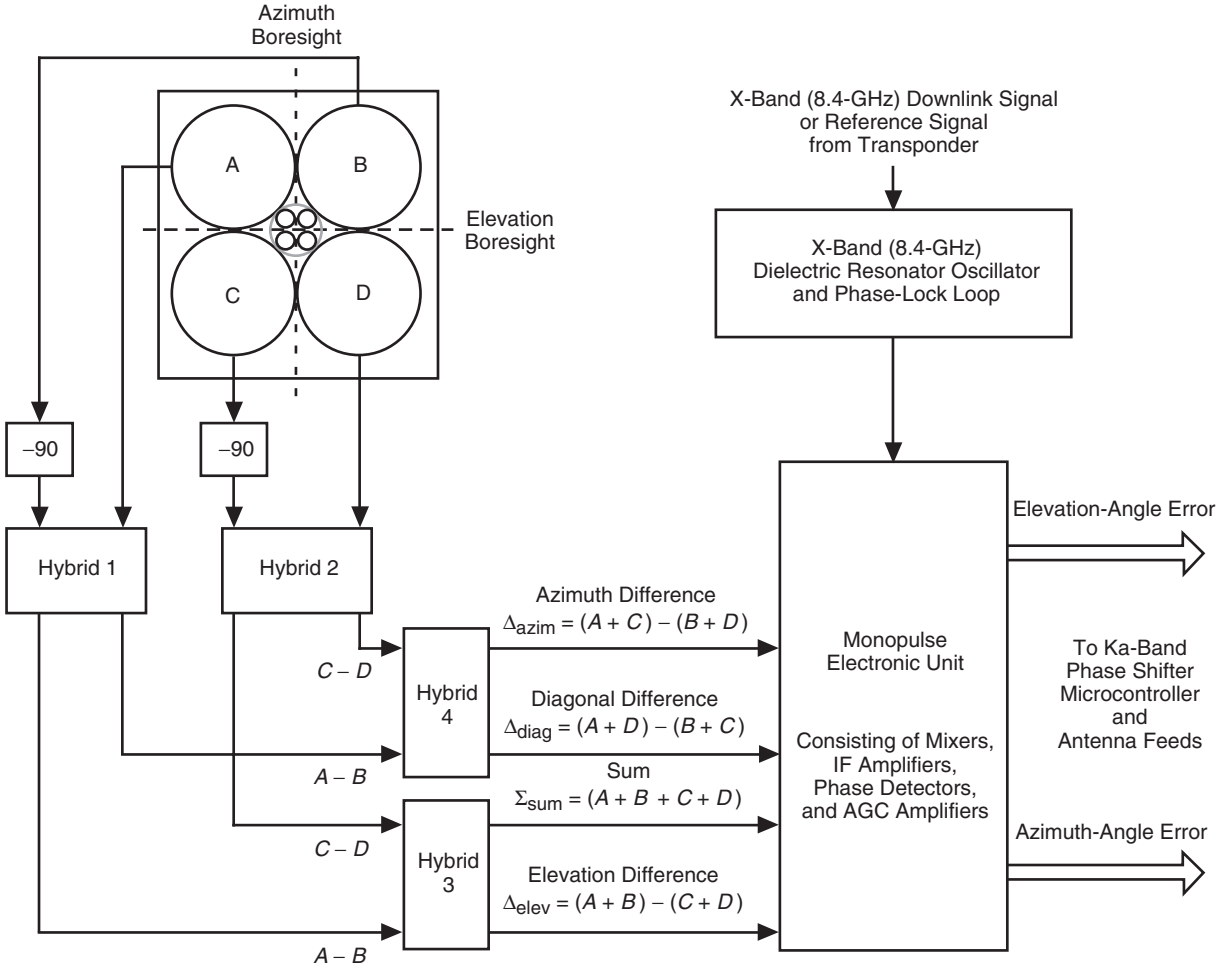

Fig. 5. X-band monopulse tracking and Ka-band pointing system.

The monopulse tracking system is designed to operate in the autonomous auto-tracking mode with an uplink X-band received signal, without the aid of the X-band downlink signal. However, it provides better precision auto-tracking when the X-band phase-tracked downlink signal (8.4 GHz) is available from the SDST. In this precision tracking mode, the DRO locks to the 8.4-GHz downlink signal from the SDST and improves the performance of the monopulse tracking system with precision tracking and higher signal-to-noise ratio (SNR). Alternatively, it is possible to use the locked voltage-controlled crystal oscillator (VCXO) signal (∼38.29 MHz) from the SDST to coherently sample and assess the tracking-angle errors.

The X-band monopulse tracking unit consists of filters, hybrids, X-band MMIC amplifiers, mixers, phase detectors, operational amplifiers (op amps), and a DRO. A common dc-to-dc converter is used for both the electronic beam-steering interface unit and the X-band monopulse tracking and Ka-band pointing subsystem. All components are commercially available, and no device development is warranted. The devices can withstand 20 krad (Si) and will require shielding for the JIMO application.

The electronic beam-steering interface shown in Figs. 4 and A-2 consists of hybrids, Ka-band MMIC linear phase shifters, MMIC amplifiers, phase comparators, op amps, a micro-controller with memory, and dc-to-dc converters. The specification of the Ka-band MMIC linear phase shifter [9] is given in Table 4. This Ka-band phase shifter needs to be developed. All other components are available. GaAs MMIC devices can withstand 1 Mrad (Si) total ionizing dosage (TID), while the remaining devices and the micro-controller circuits can withstand 20 krad and require shielding for the JIMO application.

The performance specification for the X-band monopulse tracking and Ka-band pointing subsystem is detailed in Table 5. The table also provides the preliminary evaluation of the subsystem and calculated values [10,11]. The detailed subsystem design and analysis are beyond the scope of this work. The preliminary analysis shows that the boresight rms tracking phase error is 0.21 mrad; the boresight pointing error is 0.15 mrad; and the combined boresight rms tracking and pointing error is 0.26 mrad, which is well within the specified requirement. The electronic beam-tracking and -steering system thus will meet the specified boresight beam-pointing requirement of ±3 mrad.

Table 4. Specifications for the Ka-band MMIC linear phase shifter for high-EIRP cluster-array application.

Parameter	Specification
Design frequency range	31.8 to 32.3 GHz
Bandwidth:	
−0.25 dB	32 GHz ± 500 MHz
−3 dB	32 GHz ± 1 GHz
Linear phase shift	±100 deg
Phase-shifter linearity	±4% (best straight line) to ±100 deg
Phase shift/V	50 deg to 60 deg/V, peak
Control voltage range	1 to 5 V (+3 V ± 2 V)
Insertion loss	15 dB maximum
Insertion loss flatness	±0.5 dB maximum over frequency range
	±1 dB maximum over frequency range and design temperature range
RF port return loss	15 dB minimum
RF power (1-dB compression)	+10 dBm
Design temperature range	−35 deg C to +75 deg C

Table 5. Performance specifications and estimates for X-band monopulse tracking and Ka-band pointing for cluster-antenna application.

Parameter	Specification for four-cluster antenna (1.5 m)
X-band digital monopulse tracking system	
X-band uplink frequency	7145 MHz to 7190 MHz
Typical channel (#21)	7170 MHz ± 1.5 MHz
Boresight tracking requirements	±3 mrad
Boresight tracking accuracy requirement	±0.3 mrad
Receiver antenna efficiency	45%
Antenna gain/dish	37.6 dBi, each
Antenna beamwidth	2.64 deg (46 mrad)
Antenna temperature (sun)	15 K
Tracking receiver noise figure	2.0 dB
Thermal noise power at input	−132.6 dB/Hz
Receiver channel bandwidth	20 kHz
C/N ratio at each channel	>19 dB (typical)
Minimum channel C/N required	>6 dB
Margin available	>13 dB
Dynamic range	30 dB
Thermal noise angle error: $\sigma_{S/N}$	0.07 mrad
Thermal noise bias	0.00013 mrad
Boresight randomized tracking phase quantization error: σ_Q	0.023 mrad
Phase measurement error due to tracking chain (Feed + Waveguide + LNA + AGC + LPF) + DC Converter Noise: $\sigma_{\mathrm{T-chain}}$	0.195 mrad
Total boresight rms tracking phase error: $\sigma_{\mathrm{tracking}}$	0.21 mrad
Ka-band electronic fine-beam-steering system	
Ka-band downlink frequency	32 GHz ± 10 MHz
Boresight steering requirement	±3 mrad
Boresight steering accuracy	±0.3 mrad
Pointing loss for ±0.3 mrad	0.1 dB
Antenna beamwidth	0.1826 deg (3.18 mrad)
MMIC phase-shifter range	±120 deg
MMIC phase-shifter resolution	±1 deg
Boresight randomized steering phase quantization error, σ_Q	0.022 mrad
Steering chain phase error (Hybrids + MMIC Amp + Phase Shifter + TWTA + Filter + Waveguide + Feed) + DC Converter Noise: $\sigma_{\mathrm{st-chain}}$	0.1475 mrad
Total boresight rms steering phase error, $\sigma_{\mathrm{steering}}$	0.15 mrad
Combined boresight rms tracking and steering error estimate, $\sigma_{\mathrm{combined}}$	0.26 mrad

IV. Conclusion

The study demonstrates the precise pointing and efficient spatial power-combining capabilities of an antenna cluster system. In particular, the antenna cluster meets the 10-Mbps data rate with the JIMO ±0.003-rad mechanical pointing-accuracy condition because of the electronic beam-steering capability. This preliminary design of an X-band monopulse tracking and Ka-band pointing subsystem demonstrates that the subsystem will meet the specified boresight beam-steering requirement. Additional advantages (when compared to the single, larger antenna approach) include higher antenna efficiencies, lower power density in the transmit system components, efficient spatial power combining, and a graceful degradation capability.

References

[1] *Reference for Radio Engineers*, Fourth Edition, The International Telephone and Telegraph Corporation, New York: Howard W. Sam & Co., pp. 689–698, July 1957.

[2] J. H. Yuen, ed., *Deep Space Telecommunications Systems Engineering*, Chapter 8, "Spacecraft Antennas," Y. Rahmat-Samii and G. K. Noreen, pp. 418–447, JPL Publication 82-76, Jet Propulsion Laboratory, Pasadena, California, July 1982; New York: Plenum Press, 1983; Library of Congress Catalog Number 82-084114.

[3] W. H. Kummer, "Basic Array Theory," *Proceedings of the IEEE*, vol. 80, no. 1, pp. 127–140, January 1992.

[4] A. G. Cha, "The JPL 1.5-Meter Clear Aperture Antenna With 84.5 Percent Efficiency," *The Telecommunications and Data Acquisition Progress Report 42-73, January–March 1983*, Jet Propulsion Laboratory, Pasadena, California, pp. 1–14, May 15, 1983.
http://tmo.jpl.nasa.gov/tmo/progress_report/42-73/73A.PDF

[5] J. R. Pierce and E. C. Posner, *Introduction to Communication Science and Systems*, California Institute of Technology, Pasadena, California, New York: Plenum Press, ISBN 0-306-40492-3, Third Printing, July 1985. (In particular, see Chapter 7, "Pulse Shape, Filtering and Arraying," and Section 7.8, "Antenna Arrays," pp. 166–172.)

[6] B. Cook, M. Dennis, S. Kayalar, J. Lux, and N. Mysoor, "Development of the Advanced Deep Space Transponder," *The Interplanetary Network Progress Report*, vol. 42-156, Jet Propulsion Laboratory, Pasadena, California, pp. 1–41, February 15, 2004.
http://ipnpr.jpl.nasa.gov/tmo/progress_report/42-156/156C.pdf

[7] N. R. Mysoor, S. Kayalar, J. P. Lane, and A. W. Kermode, "Performance of a Ka-Band Transponder Breadboard for Deep-Space Applications," *IEEE Aerospace Conference Proceedings*, vol. 3, Aspen, Colorado, pp. 547–557, February 1–8, 1997.

[8] M. Skolnik, *Radar Handbook*, New York: McGraw-Hill, pp. 213–224, 1970.

[9] S. Kayalar, N. R. Mysoor, and C. Andricos, "Development of Linear Phase Modulator for Spacecraft Transponding Modem," 0-7803-6599-2/01 IEEE, IEEE Aerospace Conference, Steamboat Springs, Colorado, February 2001.

[10] S. M. Sherman, *Monopulse Principles and Techniques*, Dedham, Massachusetts: Artech House, 1984.

[11] D. R. Rhodes, *Introduction to Monopulse*, New York: McGraw Hill, 1959, Reprinted by Artech House, 1980.

Appendix

JIMO Equipment List

Table A-1 includes some typical equipment necessary to produce a high-EIRP cluster array for JIMO using four antennas, each 1.5 m in diameter. The spacecraft telecommunications subsystem architecture is shown in Fig. A-1. Figure A-2 shows the high-EIRP array concept employing four 1.5-m-diameter antennas.

Table A-1. Telecommunications and high-EIRP cluster-array equipment list 1 for JIMO (four 1.5-m antenna cluster).

Equipment	Number of units	$(L \times W \times H)$ cm^3 per unit	Mass, kg	DC power, W per unit	Heritage
X-/Ka-band cluster array and telecommunication					
X-/Ka-band 1.5-m-diameter dish	4	1.5-m diam. × 1.4-m depth	30 kg	—	CloudSat
X-/Ka-band dual-feed and subreflector assembly	4	6-cm diam. × 12 cm (340 cc)	Included	—	—
X-band MGA (19 dBi)	1	15.2-cm diam. × 22.9 cm	TBD	—	MER[a]
Ka-band polarizer	4	2.5-cm diam. × 12.5 cm (78 cc)	0.16 kg	—	MER
X-band LGA	2	8.8-cm diam. × 10.2 cm	TBD	—	MRO[b]
X-band polarizer	2	2.5-cm diam. × 12.5 cm (78 cc)	0.08 kg	—	MRO
Electronic beam-steering assembly	1	12 × 12 × 20 cm (2.88 cc)	2.88 kg	14 W	New
Monopulse tracker coupler	1	4 × 5 × 10 cm (200 cc)	0.1 kg	—	New
Monopulse tracker filter	4	5 × 5 × 2.5 cm (630 cc)	1.2 kg	—	New
Ultrastable oscillator	2	10.2 × 10.2 × 10.2 cm (1060 cc)	2.1 kg	—	MER MRO
Small Deep Space Transponder with Ka-band exciter	2	17.4 × 13.4 × 14.1 cm (3.63 kg)	7.26 kg	20.6 W	MRO Ka-band exciter New
Ka-band 150-W TWTA	4	38 × 10.2 × 10.2 cm (4 kg/each) 270 W at 56%	16 kg	1350 W	New
Ka-band HVPS	4	20 × 7.1 × 9.9 cm (1406 cc)	Included	—	New
Ka-band isolator	4	8 × 1.5 × 1.7 cm (200 cc)	0.8 kg	—	MRO
X-band 100-W TWTA	2	38.1 × 6.2 × 42 cm (9921 cc) 185 W/each	6 kg	185 W	MRO
X-band HVPS	2	23 × 7 × 11 cm (1771 cc)	Included	—	MRO
X-band isolator	2	15 × 5.2 × 4.8 cm (374 cc)	0.7 kg	—	MRO
X-band waveguide transfer switch	2	11 × 5.4 × 6.8 cm (404 cc)	0.4 kg	—	MRO
Coaxial transfer switch	2	3.7 × 6 × 5.9 cm (131 cc)	0.14 kg	—	MRO
Coaxial single-pole double-throw switch	4	3.7 × 6 × 5.9 cm (131 cc)	0.28 kg	—	—
LGA downlink bandpass filter	2	5.1 × 5.1 × 2.5 cm (65 cc)	0.12 kg	—	—
X-band diplexer	2	30 × 29.2 × 10 cm (8760 cc)	1.2 kg	—	MER
X-band hybrid	1	2.5 × 1.9 × 0.3 cm (1.4 cc)	0.01 kg	—	—
Ka-band hybrid	3	2.5 × 1.9 × 0.3 cm (1.4 cc)	0.03 kg	—	—
X-band & Ka-band coaxial cables	1 lot	302 cm × 0.8-cm diam. (240 cc)	0.2 kg	—	MRO
X-band & Ka-band waveguides	1 lot	400 × 0.9 × 0.6 cm (216 cc)	0.2 kg	—	—
Radiation shielding around electronic equipment	—	TBD	TBD	—	—
Total estimate (±20%)	—	—	70.26 kg	1570 W	—

[a] Mars Exploration Rovers; [b] Mars Reconnaissance Orbiter.

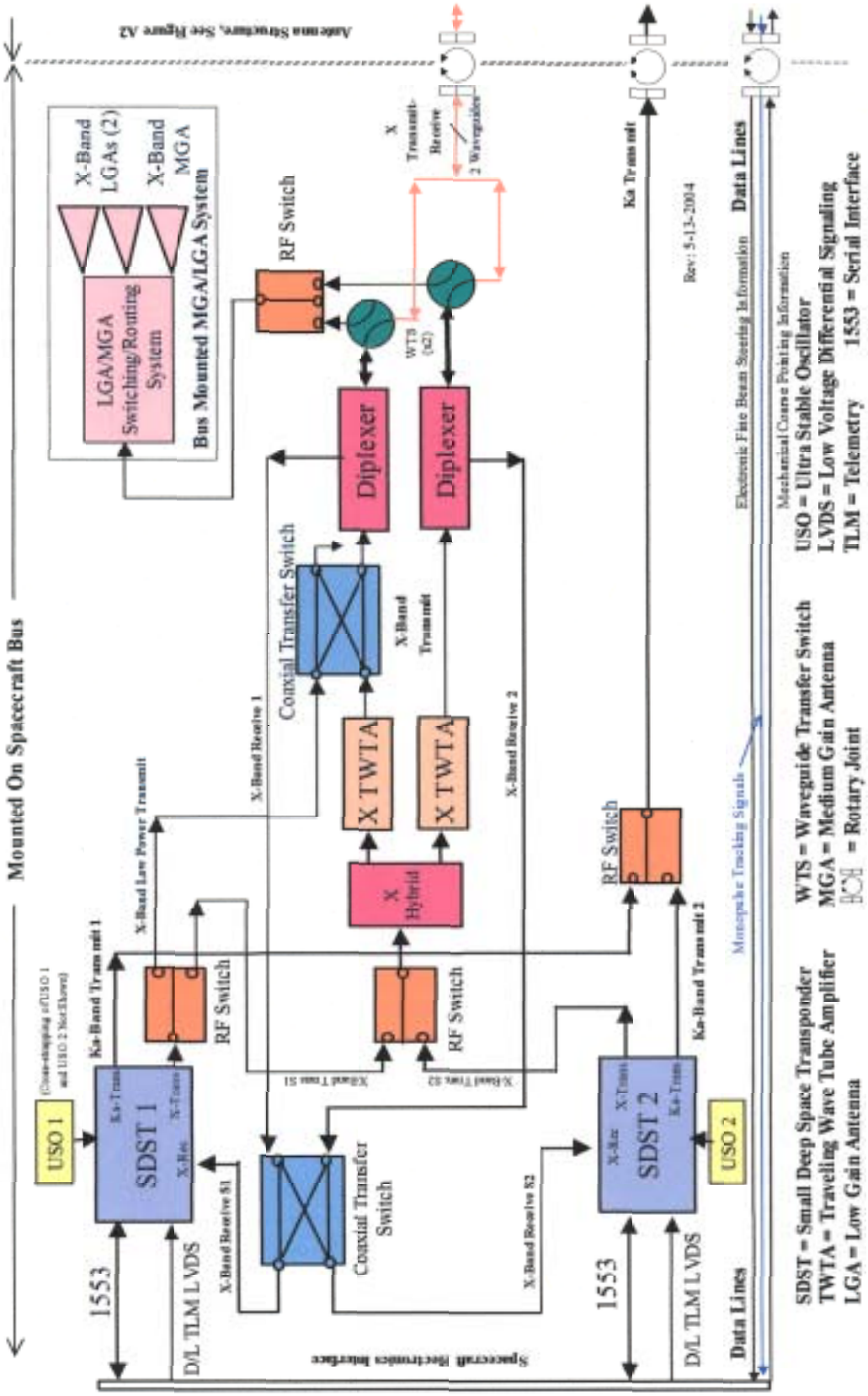

Fig. A-1. Spacecraft telecommunications subsystem architecture.

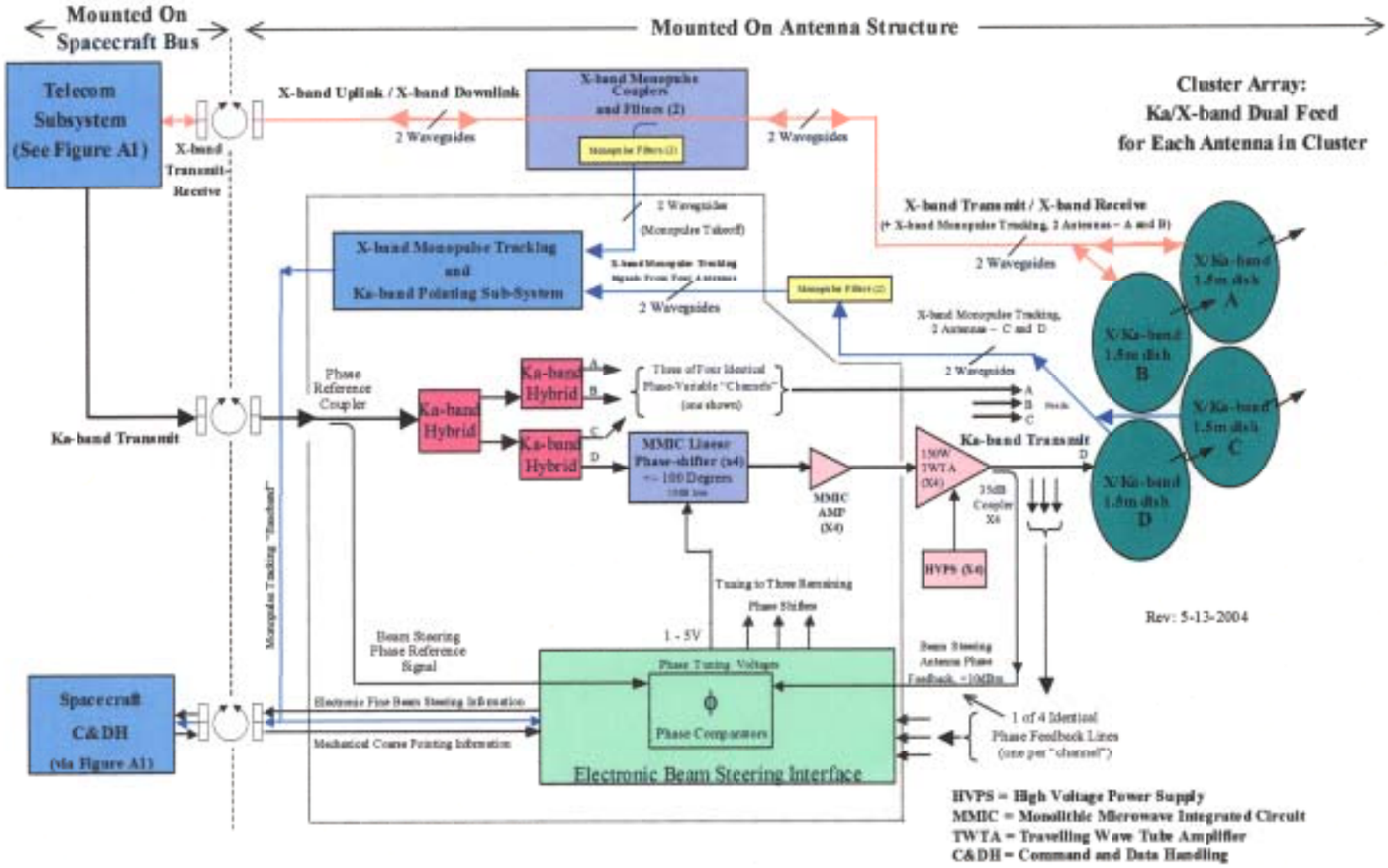

Fig. A-2. High-EIRP X-/Ka-band array concept employing four 1.5-m-diameter antennas.